

Unraveling the molecular mechanism of prion disease:Insights from α2 area mutations in human prion protein

Rongri Tan(谈荣日), Kui Xia(夏奎), Damao Xun(寻大毛), Wenjun Zong(宗文军), and Yousheng Yu(余幼胜)
Citation: Chin. Phys. B, 2023, 32 (**12**): 128703. DOI: 10.1088/1674-1056/ad08a8
Journal homepage: http://cpb.iphy.ac.cn; http://iopscience.iop.org/cpb

What follows is a list of articles you may be interested in

Bio-inspired environmental adaptability of swarm active matter

Yangkai Jin(金阳凯), Gao Wang(王高), Daming Yuan(袁大明), Peilong Wang(王培龙), Jing Wang(王璟), Huaicheng Chen(陈怀城), Liyu Liu(刘雳宇), and Xingjie Zan(昝兴杰)
Chin. Phys. B, 2023, 32 (**8**): 088703. DOI: 10.1088/1674-1056/acd688

Adsorption dynamics of double-stranded DNA on a graphene oxide surface with both large unoxidized and oxidized regions

Mengjiao Wu(吴梦娇), Huishu Ma(马慧姝), Haiping Fang(方海平), Li Yang(阳丽), and Xiaoling Lei(雷晓玲)
Chin. Phys. B, 2023, 32 (**1**): 018701. DOI: 10.1088/1674-1056/ac5c3a

Investigation of the structural and dynamic basis of kinesin dissociation from microtubule by atomistic molecular dynamics simulations

Jian-Gang Wang(王建港), Xiao-Xuan Shi(史晓璇), Yu-Ru Liu(刘玉如), Peng-Ye Wang(王鹏业),Hong Chen(陈洪), and Ping Xie(谢平)
Chin. Phys. B, 2022, 31 (**5**): 058702. DOI: 10.1088/1674-1056/ac598b

Structural and dynamical mechanisms of a naturally occurring variant of the human prion protein in preventing prion conversion

Yiming Tang(唐一鸣), Yifei Yao(姚逸飞), and Guanghong Wei(韦广红)†
Chin. Phys. B, 2020, 29 (**10**): 108710. DOI: 10.1088/1674-1056/aba9ba

Mutation-induced spatial differences in neuraminidase structure and sensitivity to neuraminidase inhibitors

Zhi-wei Yang(杨志伟), Dong-xiao Hao(郝东晓), Yi-zhuo Che(车一卓), Jia-hui Yang(杨嘉辉), Lei Zhang(张磊), Sheng-li Zhang(张胜利)
Chin. Phys. B, 2018, 27 (**1**): 018704. DOI: 10.1088/1674-1056/27/1/018704

Unraveling the molecular mechanism of prion disease: Insights from $\alpha 2$ area mutations in human prion protein

Rongri Tan(谈荣日)[1,†], Kui Xia(夏奎)[1], Damao Xun(寻大毛)[1,‡], Wenjun Zong(宗文军)[1], and Yousheng Yu(余幼胜)[2]

[1] *Department of Physics, Jiangxi Science and Technology Normal University, Nanchang* 330013, *China*
[2] *School of Science, East China University of Technology, Nanchang* 330013, *China*

(Received 16 September 2023; revised manuscript received 19 October 2023; accepted manuscript online 2 November 2023)

Prion diseases are a class of fatal neurodegenerative diseases caused by misfolded prion proteins. The main reason is that pathogenic prion protein has a strong tendency to aggregate, which easily induces the damage to the central nervous system. Point mutations in the human prion protein gene can cause prion diseases such as Creutzfeldt–Jakob and Gerstmann's syndrome. To understand the mechanism of mutation-induced prion protein aggregation, the mutants in an aqueous solution are studied by molecular dynamics simulations, including the wild type, V180I, H187R and a double point mutation which is associated with CJD and GSS. After running simulations for 500 ns, the results show that these three mutations have different effects on the kinetic properties of PrP. The high fluctuations around the N-terminal residues of helix 2 in the V180I variant lead to a decrease in hydrogen bonding on helix 2, while an increase in the number of hydrogen bonds between the folded regions promotes the generation of β-sheet. Meanwhile, partial deletion of salt bridges in the H187R and double mutants allows the sub-structural domains of the prion protein to separate, which would accelerate the conversion from PrPC to PrPSc. A similar trend is observed in both SASA and Rg for all three mutations, indicating that the conformational space is reduced and the structure is compact.

Keywords: prion protein, mutations, misfolding, molecular dynamics simulations

PACS: 87.10.Tf, 31.15.at, 87.15.R–, 87.15.kr **DOI:** 10.1088/1674-1056/ad08a8

1. Introduction

Transmissible spongiform encephalopathy (TSE), also known as prion disease, is a group of fatal degenerative diseases of the central nervous system that exist in many mammals due to prion isomerism.[1–3] At present, there is mad cow disease, scrapie in sheep, Creutzfeldt–Jakob disease (CJD) and fatal familial insomnia (FFI), Gerstmann's syndrome (GSS), kuru disease and so on.[4,5] These diseases have been found to be associated with the conformational conversion of a normal cellular prion protein (PrPC) into a misfolded pathogenic scrapie form (PrPSc), and many factors can trigger the isomerization of PrPC to PrPSc. However, the conversion mechanism of PrPC to PrPSc and the pathological interaction of prions remain unclear.[6,7]

The natural state prion protein (PrP) has an N-terminal flexible region and a C-terminal globular folding structural domain.[8] The N-terminal of the mature prion protein has no specific structure, and the C-terminal globular domain contains mainly three ordered α-helix structural regions ($\alpha 1$, $\alpha 2$, $\alpha 3$), two very short anti-parallel β strands ($\beta 1$, $\beta 2$), and a disulfide bond connecting $\alpha 2$ and $\alpha 3$.[9] It is now generally accepted that the C-terminal structural domain of PrPC begins to misfold by disrupting the region formed by the two β strands and $\alpha 1$ region and against the structural area of $\alpha 2$–$\alpha 3$. It is shown that among these structures, there are 40 mutant sites in the PrP gene encoding,[10,11] which are mainly present in the C-terminal globular domain of PrP, especially in the $\beta 2$–$\alpha 2$ loop region and the $\alpha 2$–$\alpha 3$ interhelical interface.[12,13] These pathogenic mutations result in human diseases such as CJD, FFI, and GSS. For example, San Hadzi *et al.* found that the pathogenic mutation H187R, which is closely related to GSS, can contribute to subdomain segregation and conformational transition of PrP by reducing the stability of the natural structure of prion protein.[14]

In recent years, a large number of experiments and computational simulations have reported that the key site of the conformational transition of prion proteins is in the $\alpha 2$ region, especially at the $\alpha 2$ C-terminal.[15–19] Mutation sites in this region play a crucial role in the misfolding of prion proteins. In hydrogen exchange combined mass spectrometry experiments, Laszlo *et al.* found that stabilization of the $\alpha 2$ region prevents misfolding and aggregation of PrP.[15] In NMR studies, the presence of a chemical agent will make the $\alpha 2$ C-terminal show a great deal of structural flexibility.[20] In addition, many molecular dynamics simulations have also shown the important role of the $\alpha 2$ C-terminal in the conformational transition of prion proteins. Chakroun *et al.* carried out the molecular dynamics simulations on the $\alpha 2$–$\alpha 3$ region and found a stable β-sheet structure in the protein structure.[21] A transition from α-helix to β-sheet was found at the $\alpha 2$ C-terminus during the conformational change.[16] These simulations also demonstrated that the $\alpha 2$ fragment plays an impor-

[†]Corresponding author. E-mail: rogertanr@hotmail.com
[‡]Corresponding author. E-mail: damao65@163.com

© 2023 Chinese Physical Society and IOP Publishing Ltd

tant role in prion misfolding and conformational transition.

To investigate the effects of mutations in the α2 region, molecular modeling techniques were employed to gain insights into the molecular mechanisms underlying the early induction of PrPC misfolding. In this work, two mutant sites, V180 and H187, were selected for analysis in the α2 region. Four systems were designed with these two mutant sites, including the wild-type (WT) structure, the V180I mutant (V180I), the H187R mutant (H187R) and the double mutations (Double). By comparing the properties of WT and several other mutations, such as hydrogen bonding, hydrophobic and electrostatic interactions, we aimed to understand the interactions between different systems. Our study analyzed the conformational fluctuations, hydrogen bonding, salt bridges and the changes in secondary structure during simulations. These mutations led to local changes in the natural structure of prion proteins. The purpose of this study was to explore the potential mechanism of prion diseases caused by mutations and provide valuable insights for future prion disease treatments.

2. Computational methods

In this work, the wild-type prion NMR structure (PDB ID: 1HJM)[22] was obtained from the Protein Data Bank (PDB)[23,24] with the pH of 7.0. The V180I and H187R mutations were altered by using the Pymol package to replace the corresponding residue of 1HJM. Four systems were studied here and their initial structures are shown in Fig. 1, namely WT, V180I, H187R and Double, respectively. Each system was placed in a cubic box with a minimum distance of 10 Å between the protein and the box boundary, and the TIP3P water model[25] was used to fill the cubic box. Molecular dynamics simulations of all systems were performed using the GROMACS 5.1.5 package[26] with Amber99sb-ildn force field. Then, in order to make the simulated systems electrically neutral, sodium ions were added to the systems to neutralize each system.

For each simulation, the system underwent energy minimization using the steepest descent method in 1000 steps. It was then heated up from 0 to 300 K and equilibrated at 1 bar and 300 K. Equilibrium MD simulations of 1000 ps and production MD simulations of 500 ns were performed for each system in the NPT ensemble. During the minimization of equilibration, periodic boundary conditions were applied to the x, y and z directions in the NPT ensemble. The SHARK algorithm was used for bond constraints in all simulations. The electrostatic interactions were handled by the particle mesh Ewald (PME) method[27] and the cutoff radius for Coulomb and van der Waals interactions were set to 10.0 Å and 14.0 Å, respectively.

To explore the mechanism that stabilizes the natural structure of PrPC, MD trajectories were analyzed from a structural and energetic perspective. After the simulation, we obtained the final conformation of the protein and placed it in Fig. S1. All trajectory analyses were performed in the GROMACS and VMD programs.[28] Root mean square deviation (RMSD) and root mean square fluctuation (RMSF) of the backbone atoms were monitored relative to the initial structure to assess conformational fluctuations and the stability of the MD trajectories. Then, the stability of the PrPC hydrophobic core was assessed by calculating the solvent accessible surface area (SASA) using VMD, and the radius of gyration (Rg) was used to measure the size variation of the protein. To examine inter-peptide interactions, inter-peptide backbone hydrogen bonds and salt bridges (SBs) were calculated. Furthermore, the evolution of secondary structure and the measurement of secondary structure percentage were determined throughout the simulation using the DSSP program.[29]

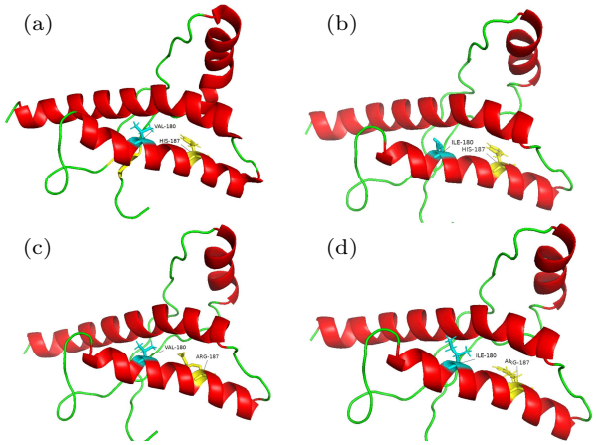


Fig. 1. Initial structure of WT PrP and its variants. (a) WT PrP, (b) V180I variant, (c) H187R variant, and (d) Double variant.

3. Results and discussion

3.1. The stability of the α2 C-terminal and the hydrophobicity of the protein.

First, the RMSD of the Cα atom in the entire sequence was calculated to examine the structural changes caused by mutations in the globular structural domain. For each system, there are three parallel runs. Run 1 is shown in Fig. 1, run 2 and run 3 are shown in Figs. S2 and S3, respectively. As shown in Fig. 2(a), the RMSD values indicated that the WT reached equilibrium at 50 ns, whereas three mutants started to stabilize at 260 ns. It was also observed that the mutations exhibited higher structural fluctuation compared to the WT. The average RMSD values in the V180I, H187R, and Double systems were 0.26 nm, 0.30 nm and 0.29 nm, respectively, while it is 0.23 nm in WT. Furthermore, the minimum deviation of the wild-type protein revealed that the wild-type conformation is the most stable, when compared to the three mutations.

To further explore the structural changes of each part, the RMSD value of α1, α2, and α3 was calculated in each system. Figures 2(c)–2(e) show the volatility of each helix in dif-

ferent systems. It can be seen from the figure that each system was relatively stable in the $\alpha1$ region. In contrast, for the $\alpha3$ area, three mutants are more flexible. Interestingly, the mutant sites of the three mutations are all located in the $\alpha2$ region. However, it has been found that the presence of a mutation at residue 187, such as H187R and Double, is more likely to cause $\alpha2$ fluctuations in the $\alpha2$ region.

The RMSF serves as an important indicator of residue mobility around its average position, and can be used to analyze the dynamic stability of proteins. In Fig. 2(b), the RMSF trends are shown to be similar in the four systems. In the H187R mutant, dynamic instability is observed in the $\beta1$–$\alpha1$ loop and $\alpha2$–$\alpha3$ loop, with maximum fluctuation of 0.50 nm and 0.54 nm. Conversely, the V180I mutant is dynamically stable for all regions of the protein. These mutations at residues 180 and 187 have led to a slight decrease in the flexibility of Double. Notably, all mutant systems have anomalous fluctuations near their mutation sites, especially $\alpha2$ C-terminal. These fluctuations are considered as the first indication of conformational transitions.[11] Therefore, it can be inferred that all mutant systems undergo conformational fluctuations, and that point mutations may affect local protein interactions required for fiber species oligomerization.[30]

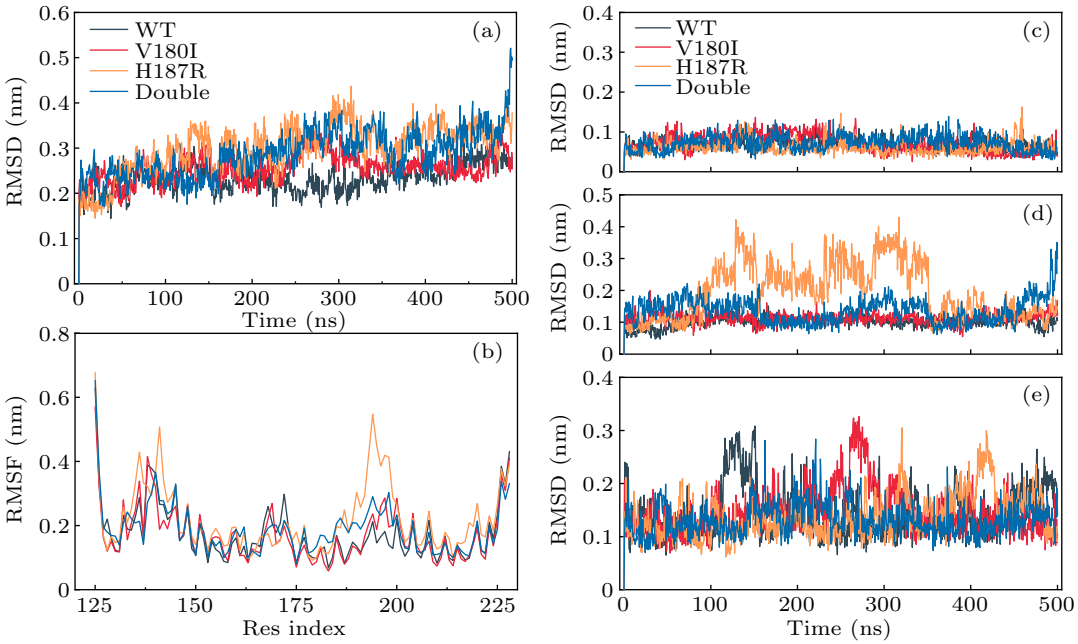


Fig. 2. Stability and rigidity of WT PrP and its variants. (a) The RMSD values and (b) RMSF values of each system. (c)–(e) The backbone RMSD of three helixs ($\alpha1$, $\alpha2$, $\alpha3$).

The time evolution of the SASA, hydrophobic SASA ($S_{\rm pho}$) and hydrophilic SASA ($S_{\rm phi}$) is depicted in Fig. 3. From the figure, we can find that the $S_{\rm phi}$ is higher than the $S_{\rm pho}$ in all systems. This phenomenon is due to the fact that hydrophobic residues and side chains of the protein can readily reside within the core, while the hydrophilic part is exposed to the solution. Furthermore, the difference between $S_{\rm pho}$ and $S_{\rm phi}$ is significantly increased in three mutant systems compared to the WT. Table 1 displays the specific solvent surface values that reveal that the $S_{\rm pho}$ of WT is 3288 Å^2, whereas the $S_{\rm pho}$ of other three mutant forms have reduced to 3238 Å^2, 3154 Å^2, and 3184 Å^2, respectively. In contrast, the $S_{\rm phi}$ has increased to different degrees during the simulation. The transformation trends of $S_{\rm phi}$ and $S_{\rm pho}$ are consistent with the study of the human prion protein.[31] It is well known that the unfolding of the protein releases hydrophobic residues, which increases the exposure hydrophobic surface. Furthermore, specific experimental results have demonstrated that protein denaturation is associated with an increase in hydrophobic surface exposure.[32,33] These results suggest that the onset of prion diseases may be related to prion protein denaturation caused by mutations.

Table 1. The average of SASA values.

System	Total (Å^2)	Hydrophobic (Å^2)	Hydrophilic (Å^2)
WT	6937	3288	3649
V180I	7009	3238	3771
H187R	6947	3154	3793
Double	6895	3184	3711

The Rg is a valuable parameter for measuring the effective size of a protein chain. Therefore, to comprehend the overall shape and size change in the mutant protein, we plot the function diagram of Rg over time and the probability distribution of Rg for Cα atom, as shown in Fig. 4. Figure 4(a) reveals that the Rg value of WT is situated at the bottom of the depicted position, with the smallest Rg value. After 300 ns evolution, the Rg value of the Double is eventually stable at the highest Rg value of 1.49 nm. This shows that the overall size of the protein is altered by the mutation. In Fig. 4(b), the

V180I mutant form is observed to have the narrowest Rg distribution, indicating that V180I has the least conformational space. Both the double point mutation and H187R have a broader distribution than V180I, while the wild type has the broadest Rg distribution. It suggests that point mutations contribute to the folded conformation of the entire protein.

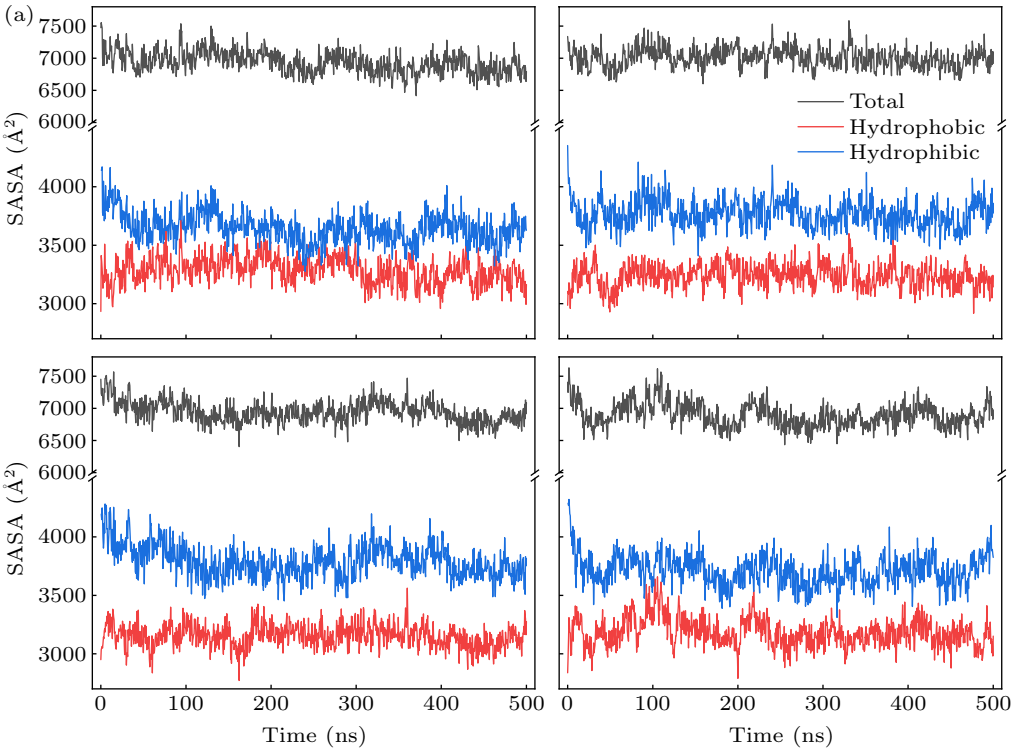


Fig. 3. Time evolutions of the solvent accessible area of (a) WT, (b) V180I, (c) H187R and (d) Double.

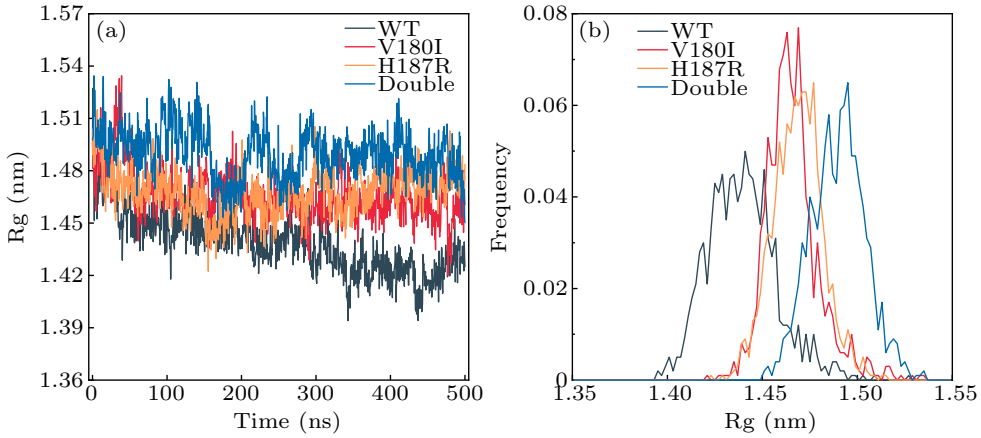


Fig. 4. (a) The Rg value vs. time. (b) The probability distribution of radius of gyration of Cα.

3.2. Local disruption of hydrogen bonds and salt bridges

Some specific salt bridges can play a decisive role in stabilizing the folded structure of PrPC.[34] Even a small disruption of salt bridge accelerates the transition of the folded conformation toward an unstable state.[35] Therefore, the probability diagram of SBs of wild type and mutant are plotted in the Fig. 5. For the α1 region, the SBs of V180I and H187R do not show significant changes. In the Double, the occupancy of D144_R148 increased abnormally, resulting in a shortened distance between the two residues and verifying the result that α1 has significant fluctuations in the Double. In the α2–α3 loop region, E196_R156 was weakened in H187R and Double, which cause the α1 structural domain to move away from the α2–α3 core. This process led to the increased exposure of the hydrophobic core to the solvent environment.[36] Additionally, the salt bridges of D178_R164 and D202_R156 were partially lost in H187R and Double, causing the two substructural domains, β1–α1–β2 and α2–α3, to separate. For E207_K204 and E211_K204 in the α3 region, all three mutant systems experienced the total or partial loss, leading to instability in the α3 region. These mutations disrupted the native salt bridge network and potentially accelerated the conversion of PrPC to PrPSc, which may explain the occurrence of the disease.

To better understand the stability of each domain, the

main chain hydrogen bonds of each domain are listed in Tables 2 and 3. The occupancy of hydrogen bonds over 75% is considered to be real. In Table 2, it can be observed that although the number of hydrogen bonds in the $\alpha1$ region did not change for all four systems, the 144Asp–148Arg, which is found in all other systems, was not found in Double. And the distance of Double between 144Asp and 148Arg is shortened in salt bridge, which may also be the reason for the disruption of the hydrogen bonds. Moreover, the number of hydrogen bonds of V180I decreases significantly in the $\alpha2$ region. Additionally, the mutant forms in the $\alpha3$ region are deficient in the number of hydrogen bonds to some extent. These results indicate that the mutant forms have unstable structures in the $\alpha3$ region, consistent with the finding of salt bridges. In Table 3, more hydrogen bond interactions are found in V180I between $\beta1$ and $\beta2$, as shown by the secondary structure content later, which is the reason for the increase of β-sheet.

In addition, it was shown that short β-sheet plays an important role in the conversion of natural prion proteins into pathogenic structures, with both elongation and depletion of β-sheet likely to be key processes.[37] 129N:163O, 129O:163N, 131N:161O, and 134N:159O, the four main-chain hydrogen bonds, are believed to provide supporting evidence for the presence of naturally occurring β-sheet structures.[38] Figure 6(a) shows the occupancy of these four hydrogen bonds over time. The most significant change was observed in the hydrogen bond between 159O:134N, which showed an extremely weak appearance in V180I compared to the WT. The change may be due to the elongation of the β structure (Table 2), causing disruption in the original hydrogen bond. On the other hand, in Double, where residue 180 is also replaced, the 159O:134N hydrogen bond is strengthened. This may be due to the mutation of residue 187 that stabilizes the presence of the hydrogen bond. However, for the rest of the hydrogen bonds in the four systems, no significant change in hydrogen bond occupancy was observed.

Table 2. The hydrogen bonds of helix areas.

Area	WT	V180I	H187R	Double
$\alpha1$	144 Asp O–H Arg 148 144 Asp O–H Arg 148 143 Ser O–H Asp 147 147 Asp O–H Ser 143	146 Glu O–H Tyr 159 146 Glu O–H Tyr 159 144 Asp O–H Arg 148 150 Tyr O–H Glu 146	147 Asp O–H Arg 151 147 Asp O–H Arg 151 146 Glu O–H Tyr 159 151 Arg O–H Asp 147	153 Asn O–H Arg 156 153 Asn O–H Arg 156 147 Asp O–H Arg 151 156 Arg O–H Asn 153
$\alpha2$	179 Cys O–H Thr 183 180 Val O–H Ile 184 181 Asn O–H Lys 185 182 Ile O–H Gln 186 183 Thr O–H His 187 184 Ile O–H Thr 188 188 Thr O–H Thr 192	174 Asn O–H Asp 178 180 Val O–H Ile 184 181 Asn O–H Lys 185 183 Thr O–H His 187 184 Ile O–H Thr 188	180 Val O–H Ile 184 181 Asn O–H Lys 185 182 Ile O–H Gln 186 183 Thr O–H His 187 184 Ile O–H Thr 188 185 Lys O–H Val 189 188 Thr O–H Thr 192	178 Asp O–H Asn 174 184 Ile O–H Ile 180 185 Lys O–H Asn 181 186 Gln O–H Ile 182 187 Arg O–H Thr 183 189 Val O–H Lys 185 192 Thr O–H Thr 188
$\alpha3$	202 Asp O–H Met 206 203 Val O–H Glu 207 206 Met O–H Val 210 207 Glu O–H Glu211 208 Arg O–H Gln 212 209 Val O–H Met 213 210 Val O–H Cys 214 211 Glu O–H Ile 215 212 Gln O–H Thr 216 213 Met O–H Gln 217 214 Cys O–H Tyr 218 215 Ile O–H Glu 219	202 Asp O–H Met 206 203 Val O–H Glu 207 205 Met O–H Val 209 206 Met O–H Val 210 207 Glu O–H Glu211 211 Glu O–H Ile 215 214 Cys O–H Thr 218 217 Gln O–H Glu 221 218 Tyr O–H Ser 222 221 Glu O–H Tyr 225	202 AspO–H Met 206 206 Met O–H Val 210 209 Val O–H Met 213 210 Val O–H Cys 214 211 Glu O–H Ile 215 213 MetO–H Gln 217 214 Cys O–H Tyr 218 217 Gln O–H Glu 221 218 Tyr O–H Ser 222 221 Glu O–H Tyr 225	205 Met O–H Thr 201 206 Met O–H Asp 202 207 Glu O–H Val 203 210 Val O–H Met 206 211 Glu O–H Glu 207 214 Cys O–H Val 210 218 Tyr O–H Cys 214 221 Glu O–H Gln 217 222 Ser O–H Tyr 218

Table 3. The hydrogen bonds of special sites.

Area	WT	V180I	H187R	Double
$\beta1$–$\beta2$	129 Met O–H Tyr 163 161 Val O–H Gly 131 163 Tyr O–H Met 129	129 Met O–H Tyr 163 131 Gly O–H Val 161 161 Val O–H Gly 131 163 Tyr O–H Met 129	129 Met O–H Tyr 163 161 Val O–H Gly 131 163 Tyr O–H Met 129	129 Met O–H Tyr 163 131 Gly O–H Val 161 163 Tyr O–H Met 129
$\beta2$–$\alpha2$ loop	165 Pro O–H Tyr 169	165 Pro O–H Glu 168	165 Pro O–H Glu 168 172 Gln O–H Val 176	165 Pro O–H Tyr 169

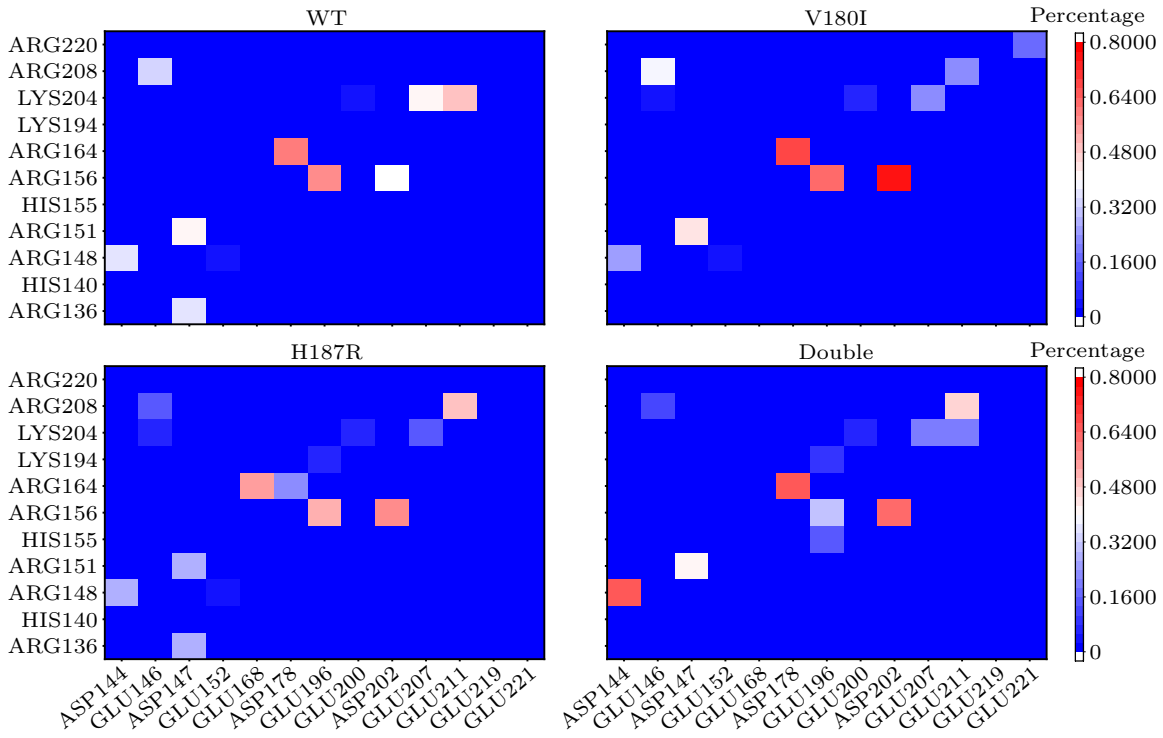


Fig. 5. The salt-bridge heatmap of (a) WT, (b) V180I, (c) H187R and (d) Double.

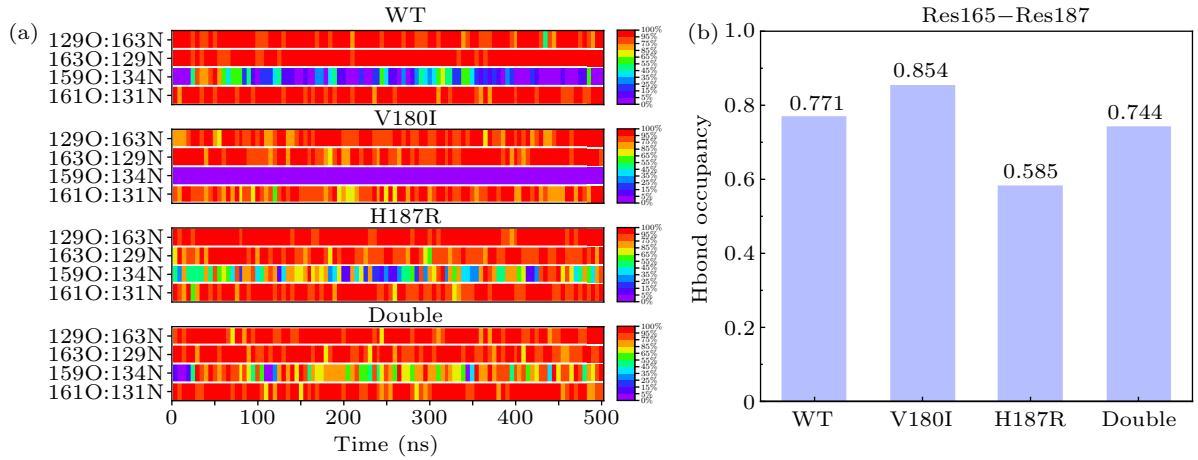


Fig. 6. (a) Occupancy plots of different hydrogen bond pairs present in S1 and S2 strand of each system. (b) Occupancy plot of Res165–Res187 hydrogen bond.

The mutant protein undergoes some local conformational changes relative to the natural protein, especially near the mutation site. It can be seen from Fig. 6(b) that the replacement of His187 with Arg187 results in the repulsion between Arg187 and Arg156 due to their positively charged side chains. This repulsion is influenced by strong electrostatic interactions. As a result, Arg187 experienced a significant deviation from Arg156, leading to an increase in the distance between these two residues. Figure 6(b) illustrates the bonding interaction of residues 165 and 187, whereby there is a significant decrease in H187R, indicating that Arg156 and Arg187 move apart from each other. This increased distance creates a gap in the protein region, thus exposing more protein sections to the solvent. Similarly, in the Double, the bonding between residue 165 and residue 187 is strengthened compared to H187R. This effect can be attributed to the mutation of residue 180, which facilitates the interaction between residues. In summary, it is not difficult to draw that Double has a slight inhibitory effect on the disruption of single point mutations (V180I and H187R).

3.3. The secondary structure of the protein

Here, in order to obtain detailed structural information of PrP in the four systems, secondary structure analysis is performed for all systems, and the results are shown in Figs. 7 and 8. It can be observed from Fig. 7 that WT and other mutations rarely change the natural structure of PrP, but they are easy to transform into disordered irregularly coil and turn at the $\alpha 2$ C-terminus. Previous studies have shown that the C-terminus of $\alpha 2$ is highly capable of forming β-sheet,

and that stabilizing this region can prevent the misfolding and oligomerization of PrP.[39,40] Interestingly, Fig. 7(b) reveals that V180I is unstable in the α2 region, causing it to extend into β-sheet formation. This observation highlights a negative correlation between the stability of α22 and the propensity for structural misfolding.

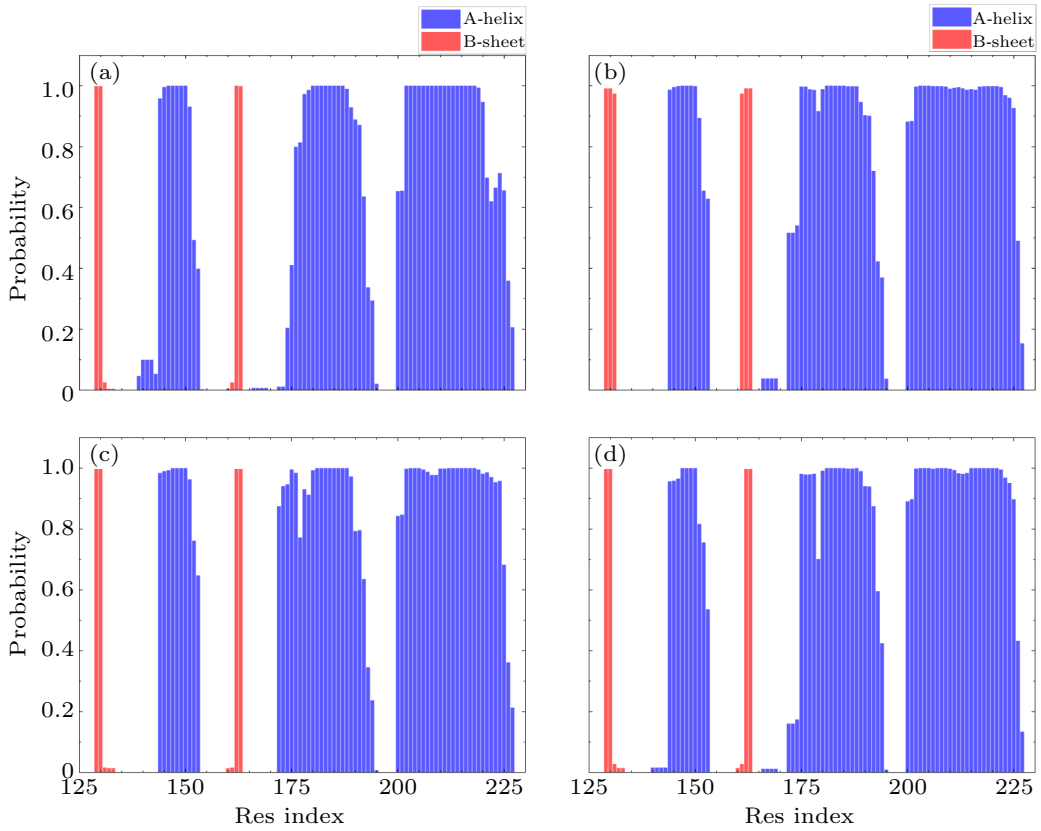


Fig. 7. The probability of each residue for helix and sheet of (a) WT, (b) V180I, (c) H187R and (d) Double.

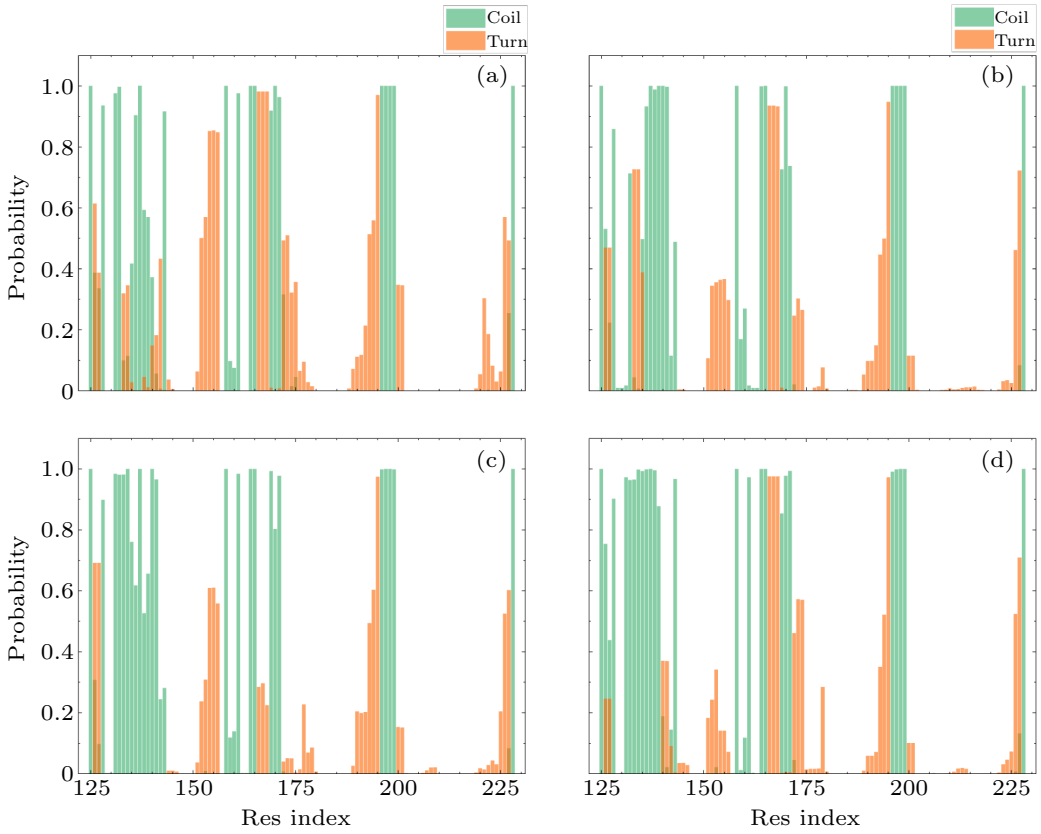


Fig. 8. The probability of each residue for coil and turn of (a) WT, (b) V180I, (c) H187R and (d) Double.

In Fig. 8, the $\beta1$–$\alpha1$ structural domains of all three mutations tend to form the irregular coil compared with the $\beta1$–$\alpha1$ region of the wild type. In Fig. 9, we observed that the total content of random coils increased from 22% to 23% and 24% in H187R and Double, respectively. Furthermore, the content of turns in all helical regions decreased in all three mutant systems because partial turn structures were transformed into a helical structure due to the mutations, especially in the $\alpha3$ region. In comparison to the WT, a significant increase in the content of the α-helix was observed in the three mutant systems. This observation can be seen in Fig. 9. Meanwhile, the content of turn was reduced from 15% to 12%, 9%, and 11%, respectively. This result suggested that mutations at the $\alpha2$ C-terminus play a key role in the transformation of the natural structure, and it also demonstrated that the $\alpha2$ C-terminus is unstable.

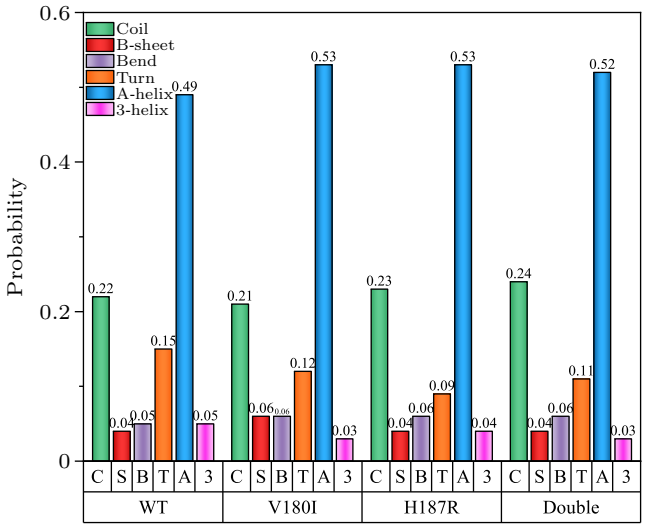


Fig. 9. The average content of different secondary structures of each system.

4. Conclusion

The all-atom MD simulations were performed to investigate the effects and kinetic properties of mutations in the $\alpha2$ region on the PrP structure, aiming to understand the molecular basis of disease-associated structural transitions. Although the differences between mutants and WT are usually limited, three mutations had distinct effects on the kinetics properties of PrP. Specifically, compared to other mutations, V180I resulted in the formation of an extended β-sheet in the secondary structure and an increased number of hydrogen bonds in the connection area of $\beta1$–$\beta2$. It also destabilized the $\alpha2$ region, leading to a significant reduction in the number of hydrogen bonds on $\alpha2$. In H187R and Double, key salt bridges such as E196_R156 and D178_R156 were weakened or disappeared, causing the $\alpha2$ structural domain to become isolated from the others and exposing more residues to the solvent. The measurements of Rg and SASA indicated that several mutations induce minor conformational changes during the simulation. Therefore, we proposed that even small changes in natural proteins may be sufficient to trigger self-aggregation and cause diseases.

Data and software availability

The calculations and analysis of RMSD, RMSF, Rg, DSSP, salt bridges and Hbonds were performed with Gromacs software (https://www.gromacs.org/) version 5.1.5. The protein structure is available on Github (https://github.com/xk20/MMi-data-prion-validation/).

Acknowledgments

Project supported by the National Natural Science Foundation of China (Grant Nos. 52073128, 12164002, and 11964012), the Foundation of Educational Committee of Jiangxi Province of China (Grant No. GJJ211112), and the Fund for Distinguished Young Scholars of Jiangxi Science & Technology Normal University (Grant No. 2015QNBJRC002).

References

[1] Yoshida S and Hasegawa T 2022 *Neurochem. Int.* **155** 105307
[2] Brandel J P 2022 *Rev. Med. Interne* **43** 106
[3] Lambert Z J, Greenlee J J and Cassmann E D 2021 *Viruses* **13** 12
[4] Prusiner S B 1998 *Proc. Natl. Acad. Sci. USA* **95** 13363
[5] Collinge J 2004 *Annu. Rev. Neurosci.* **24** 519
[6] Palaniappan C, Narayanan R C and Sekar K 2021 *ACS Chem. Neurosci.* **12** 2810
[7] Zhou S, Liu X, An X, Yao X and Liu H 2017 *ACS Chem. Neurosci.* **8** 2446
[8] Singh R K, Chamachi N G and Chakrabarty S 2017 *J. Phys. Chem. B* **121** 550
[9] Xu Z, Liu H, Wang S, Zhang Q, Yao X, Zhou S and Liu H 2020 *ACS Chem. Neurosci.* **11** 772
[10] Guo J, Ning L, Ren H, Liu H and Yao X 2012 *Biochim. Biophys. Acta* **1820** 116
[11] Rossetti G, Cong X, Caliandro R, Legname G and Carloni P 2011 *J. Mol. Biol.* **411** 700
[12] Scheckel C and Aguzzi A 2018 *Nat. Rev. Genet.* **19** 405
[13] Chakroun N, Fornili A, Prigent S, Kleinjung J, Dreiss C A, Rezaei H and Fraternali F 2013 *J. Chem. Theory Comput.* **9** 2455
[14] Hadzi S, Ondracka A, Jerala R and Hafner-Bratkovic I 2015 *FASEB J.* **29** 882
[15] Singh J, Kumar H, Sabareesan A T and Udgaonkar J B 2015 *J. Am. Chem. Soc.* **136** 16704
[16] Dima R I and Thirumalai D 2015 *Proc. Natl. Acad. Sci. USA* **101** 15335
[17] Lu X, Wintrode P L and Surewicz W K 2007 *Proc. Natl. Acad. Sci. USA* **104** 1510
[18] Cobb N J, Sonnichsen F D, McHaourab H and Surewicz W K 2007 *Proc. Natl. Acad. Sci. USA* **104** 18946
[19] Kovacs G G, Trabattoni G, Hainfellner J A, Ironside J W, Knight R S and Budka H 2007 *J. Neurol.* **249** 1567
[20] Hosszu L L, Wells M A, Jackson G S, Jones S, Batchelor M, Clarke A R, Craven C J, Waltho J P and Collinge J 2005 *Biochemistry* **44** 16649
[21] Zahn R, Liu A, Luhrs T, Riek R, von Schroetter C, Lopez Garcia F, Billeter M, Calzolai L, Wider G and Wuthrich K 2000 *Proc. Natl. Acad. Sci. USA* **97** 145
[22] Calzolai L and Zahn R 2003 *J. Biol. Chem.* **278** 35592
[23] Deshpande N, Addess K J, Bluhm W F, Merino-Ott J C, Townsend-Merino W, Zhang Q, Knezevich C, Xie L, Chen L, Feng Z, Green R K, Flippen Anderson J L, Westbrook J, Berman H M and Bourne P E 2005 *Nucleic Acids Res.* **33** D233
[24] Rose P W, Beran B, Bi C, *et al.* 2011 *Nucleic Acids Res.* **39** D392

[25] Jorgensen W L, Chandrasekhar J, Madura J D, Impey R W and Klein M L 1983 *J. Chem. Phys.* **79** 926
[26] Van Der Spoel D, Lindahl E, Hess B, Groenhof G, Mark A E and Berendsen H J 2005 *J. Comput. Chem.* **26** 1701
[27] Darden T, York D and Pedersen L 1993 *J. Chem. Phys.* **98** 10089
[28] Humphrey W, Dalke A and Schulten K 1996 *J. Mol. Graph. Model.* **14** 33
[29] Kabsch W and Sander C 1983 *Biopolymers* **22** 2577
[30] Gao Y, Zhu T, Zhang C, Zhang Z H and Mei Y 2018 *Chem. Phys. Lett.* **706** 594
[31] Gu W, Wang T, Zhu J, Shi Y and Liu H 2018 *Biophys. Chem.* **104** 79
[32] Chong S H, Lee C, Kang G, Park M and Ham S 2011 *J. Am. Chem. Soc.* **133** 7075
[33] Guo J J, Ren H, Ning L L, Liu H X and Yao X J 2012 *J. Struct. Biol.* **178** 225
[34] Adrover M, Pauwels K, Prigent S, Chiara C, Xu Z, Chapuis C, Pastore A and Rezaei H 2010 *J. Biol. Chem.* **285** 21004
[35] Zhang J 2011 *J. Theor. Biol.* **269** 88
[36] Lee S, Antony L, Hartmann R, Knaus K J, Surewicz K, Surewicz W K and Yee V C 2010 *EMBO J.* **29** 251
[37] Chen W, van der Kamp M W and Daggett V 2014 *Biophys. J.* **106** 1152
[38] Cobb N J and Surewicz W K 2009 *Biochemistry* **48** 2574
[39] Knaus K J, Morillas M, Swietnicki W, Malone M, Surewicz W K and Yee V C 2001 *Nat. Struct. Biol.* **8** 770
[40] Bjorndahl T C, Zhou G P, Liu X, Perez-Pineiro R, Semenchenko V, Saleem F, Acharya S, Bujold A, Sobsey C A and Wishart D S 2011 *Biochemistry* **50** 1162